J Biochem 130, 191–198 (2001)

X-Ray Absorption Spectroscopic Analysis of the High-Spin Ferriheme Site in Substrate-Bound Neuronal Nitric-Oxide Synthase[1]

Nathaniel J. Cosper,* Robert A. Scott,*,[2] Hiroyuki Hori,† Takeshi Nishino,† and Toshio Iwasaki†,[2]

*Department of Chemistry, University of Georgia, Athens, GA 30602-2556, USA; and †Department of Biochemistry and Molecular Biology, Nippon Medical School, 1-1-5 Sendagi, Bunkyo-ku, Tokyo 113-8602

Received March 27, 2001, accepted April 17, 2001

Nitric oxide synthase (NOS) catalyzes the conversion of L-arginine to citrulline and nitric oxide through two stepwise oxygenation reactions involving N^{ω}-hydroxy-L-arginine, an enzyme-bound intermediate. The N^{ω}-hydroxy-L-arginine- and arginine-bound NOS ferriheme centers show distinct, high-spin electron paramagnetic resonance signals. Iron X-ray absorption spectroscopy (XAS) has been used to examine the structure of the ferriheme site in the N^{ω}-hydroxy-L-arginine-bound full-length neuronal NOS in the presence of (6*R*)-5,6,7,8-tetrahydro-L-biopterin. Iron XAS shows that the high-spin ferriheme sites in the N^{ω}-hydroxy-L-arginine- and arginine-bound forms are strikingly similar, both being coordinated by the heme and an axial thiolate ligand, with an Fe–S distance of *ca.* 2.29 Å. Cu^{2+} inhibition slightly affects the spin-state equilibrium, but causes no XAS-detectable changes in the immediate ferriheme coordination environment of neuronal NOS. The structure and ligand geometry of the high-spin ferriheme in arginine-bound neuronal NOS are essentially identical to those of the N^{ω}-hydroxy-L-arginine–bound form and only slightly affected by the divalent cation inhibitor of consitutive NOS.

Key words: electron paramagnetic resonance spectroscopy, heme, neuronal nitric oxide synthase, nitric oxide synthase, X-ray absorption spectroscopy.

Nitric oxide (NO) serves as a physiological vasodilator, neurotransmitter, and cytostatic agent in mammalian cells, and is generated by a family of enzymes termed nitric oxide synthases (NOSs) (*1–5*). All known NOS isoforms are each catalytically active as a homodimeric, bidomain flavo-hemeprotein, consisting of a flavin-containing C-terminal reductase domain and a heme-containing N-terminal oxygenase domain (*6–9*). The oxygenase domain also contains binding sites for 6(*R*)-5,6,7,8-tetrahydro-L-biopterin (H_4BP), L-arginine, and an interdomain binding site for a tetrathiolate zinc center (*10–13*). During NO synthesis, the two flavins (FAD and FMN) in the reductase domain mediate electron transfer from NADPH to the heme group in the oxygenase domain, where oxygen binding and activation take place (*1, 6, 14–16*). Spectroscopic studies on the heme centers of the NOS isoforms involving absorption, electron paramagnetic resonance (EPR), resonance Raman, and magnetic circular dichroism techniques, along with mutational analysis, have suggested that an endogenous thiolate sulfur donor ligand is coordinated to the central heme iron, as in the cases of cytochrome P450 and chloroperoxidase (*17–26*).

Neuronal NOS (nNOS) generates NO through the two-step oxygenation reactions that convert L-arginine to citrulline. Its activity is dependent on oxygen, NADPH, H_4BP, and Ca^{2+}-calmodulin (*1, 6, 14*). The first step is the formation of N^{ω}-hydroxy-L-arginine (NOHA) as an enzyme-bound intermediate (*1, 14, 27*). It has been proposed, by analogy to P450 mechanisms, that the conversion of L-arginine to NOHA requires reduction of the ferriheme, binding of O_2 to form the ferrous-O_2 adduct, and activation of O_2 to form a reactive high-valent oxo-ferryl porphyrin, a π-cation radical species which allows oxygen insertion into L-arginine (*1, 14, 28*) The second step, *i.e.* conversion of NOHA to citrulline and NO, is thought to require the binding of O_2 to the ferrous enzyme, and the involvement of the ferric peroxide intermediate and an NO-L-arginine radical to form a putative iron-peroxo-NOHA radical intermediate (*1, 14, 28*). Although a possible two-step oxygenation mechanism for NOS has been proposed on the basis of analogy to P450-*N*-hydroxylation and P450-aromatase systems, there are sub-

[1] This investigation was supported in part by Grants-in-Aid for Scientific Research on Priority Areas from the Ministry of Education, Science, Sports and Culture of Japan ("Biometallics" 08249104 to TN and "Biomachinery" 11169237 to TI), Grants-in-Aid from the Ministry of Education, Science, Sports and Culture of Japan (09480167 to TN, and 8780599 and 11780455 to TI), and by the National Institutes of Health (GM 42025 to R.A.S.) The XAS data were collected at SSRL, which is operated by the Department of Energy, Division of Chemical Sciences. The SSRL Biotechnology program is supported by the National Institute of Health, Biomedical Technology Program, Division of Research Resources

[2] To whom correspondence should be addressed Robert A. Scott, Phone +1-706-542-2726, Fax: +1-706-542-9454, E-mail rscott@uga.edu, Toshio Iwasaki, Phone +81-3-3822-2131 (Ext 5216), Fax +81-3-5685-3054, E-mail iwasaki@biochem.om.nms.ac.jp

Abbreviations eNOS, endothelial nitric oxide synthase, EPR, electron paramagnetic resonance, EXAFS, extended X-ray absorption fine structure; FT, Fourier transform; H_4BP, (6*R*)-5,6,7,8-tetrahydro-L-biopterin, iNOS, inducible nitric oxide synthase, NO, nitric oxide, NOHA, N^{ω}-hydroxy-L-arginine; NOS, nitric oxide synthase, nNOS, neuronal nitric oxide synthase; SSRL, Stanford Synchrotron Radiation Laboratory; XAS, X-ray absorption spectroscopy

tle differences between NOS isoforms and cytochromes P450, which suggest that the NOS reaction may be more complex. First, there is little homology in amino acid sequence or overall protein folding between the NOS oxygenase domain and cytochrome P450, thereby excluding NOS from the cytochrome P450 gene family All NOS isoforms are each catalytically active only as a homodimer (*1, 6, 8, 29*), and mutagenesis studies have indicated that appropriate cross-talk between the N-terminal hook region and the substrate-binding distal pocket of NOS isoforms is essential for proper activation and regulation of the citrulline- and NO-forming activity (*12, 30–32*). Second, all NOS isoforms show an absolute requirement of H_4BP for NO synthase activity (*33, 34*). The exact role of H_4BP in NOS catalysis remains controversial. Recent studies have suggested a possible redox function for the H_4BP cofactor (*13, 35, 36*), but the redox cycling of H_4BP in the NOS catalytic cycle seems to be different from that observed with the aromatic amino acid hydroxylase reaction, which requires a non-heme iron center in close proximity to H_4BP (*13, 36*).

To fully understand the mechanism of NO synthesis, it is essential to determine the changes that the catalytic center undergoes during the reaction cycle (*28, 37*). The iron coordination structures of a variety of heme proteins including cytochromes P450 and chloroperoxidase have been studied by X-ray absorption spectroscopy (XAS) (*37–40*). The metal-ligand bond distances obtained by XAS and high-resolution X-ray crystallographic analysis are in close agreement for several different oxidation and spin states of cytochrome P450 (*37*). Extensive XAS analyses have been conducted with cytochromes P450 and chloroperoxidase to elucidate the change in the iron coordination in relation to the catalytic mechanism and to elucidate the structures of stable intermediate species (*37–42*). Although several X-ray crystal structures of eNOS and iNOS oxygenase domains complexed with substrate and inhibitors have been reported recently (*10–13, 43*), the NOS holoprotein is a complex, multidomain flavohemoprotein whose flavin and heme centers are probably positioned near each other (*21*). No detailed structural information on the heme site has been obtained for full-length NOS isoforms, and no XAS studies on any oxidation or spin state of any NOS isoform have been reported so far. As an initial step toward understanding the structural changes of the heme site during the catalysis of NOS isoforms, we report herein XAS analysis of the ferriheme site of substrate-bound full-length nNOS. We also examine the heme site structure of nNOS upon binding a divalent cation inhibitor, Cu^{2+}, that strongly blocks the NOS activity of constitutive NOS isoforms (*44–46*), and may have an impact on controlling NOS and guanylyl cyclase activity in mammalian cells.

EXPERIMENTAL PROCEDURES

Calmodulin, FAD, FMN, L-Arg, and L-citrulline were from Sigma Chemicals, and 6(*R*)-5,6,7,8-tetrahydro-L-biopterin (H_4BP) was obtained from the Schircks Laboratories (Jona, Switzerland). [^{14}C-*U*]-L-Arg was obtained from Dupont, New England Nuclear. 2′,5′-ADP Sepharose 4B, Sephacryl S-300HR, and DEAE Sepharose Fast Flow were purchased from Pharmacia Biotech, and Ampure SA from Amersham Life Science. Water was purified with a Milli-Q purification system (Millipore). Other chemicals used in this study were of analytical grade.

A heterologous expression system for the full-length wild-type nNOS in *Escherichia coli* was constructed with the pCWori+ vector (*47–49*) and the chaperonin expression vector pKY206 (pACYC184; Nippon Gene, Toyama) carrying the *E. coli* chaperonin *groELS* genes (kindly provided by Dr. K. Ito, Kyoto University), as reported previously (*31*). The recombinant nNOS produced in *E. coli* strain BL21 was purified on ice or at 4°C essentially as described in the literature (*49*), except that purification was conducted by 2′,5′-ADP Sepharose 4B column chromatography (Amersham Pharmacia Biotech), followed by Sephacryl S300HR and DEAE Sepharose Fast Flow column chromatography (Amersham Pharmacia Biotech) (*31*), and that the overnight dialysis step was omitted. H_4BP (30 μM) and L-arginine (1 mM) were supplied during the purification. The catalytic activity and purity of the purified enzyme were comparable to those previously reported for recombinant nNOS by others (*49*).

NOS activity was measured by monitoring the conversion of [^{14}C-*U*]-L-Arg to [^{14}C-*U*]-L-citrulline, as described previously (*50*). The standard assay was performed at 25°C in an assay mixture containing 16.7 mM HEPES-NaOH buffer, pH 7.4, 4.2 mM Tris-HCl buffer, pH 7.4, 667 μM EDTA, 167 μM EGTA, 667 μM DTT, 16.7 μM [^{14}C-*U*]-L-Arg, 667 μM NADPH, 1.2 mM $CaCl_2$, 6.7 μg of calmodulin, 1.25 μM FAD, 1.25 μM FMN, 2.5 μM H_4BP and the enzyme, in a total volume of 30 μl. The specific activity of [^{14}C-*U*]-L-Arg used in the assays was 11.84 GBq/mmol.

Absorption spectra were recorded with a Hitachi U3210 spectrophotometer or a Beckman DU-7400 spectrophotometer. Electron paramagnetic resonance (EPR) spectra of several different batches of purified nNOS were measured at JEOL, Tokyo, with a JEOL JES-TE200 spectrometer equipped with an ES-CT470 Heli-Tran cryostat system, in which the temperature was monitored with a Scientific Instruments digital temperature indicator/controller Model 9650 and the magnetic field was monitored with a JEOL NMR field meter ES-FC5. EPR spectroscopic measurements were also carried out with a JEOL JEX-RE1X spectrometer equipped with an Air Products model LTR-3 Heli-Tran cryostat system, in which the temperature was monitored with a Scientific Instruments series 5500 temperature indicator/controller, as reported previously (*51*). All EPR data were processed with KaleidaGraph software ver. 3.05 (Abelbeck Software).

XAS data were collected at the Stanford Synchrotron Radiation Laboratory (SSRL) with the SPEAR storage ring operating in a dedicated mode at 3.0 GeV (Table I). The iron concentrations in the samples for XAS measurement were ~1 mM. The XAS samples were prepared as outlined for bacterial cytochrome aa_3 (*52*) with the following modifications. Purified nNOS preincubated with 10 mM substrate (L-arginine or NOHA) and 1 mM H_4BP on ice in either the presence or absence of $CuCl_2$ was immediately precipitated with 40 mM potassium phosphate buffer, pH 7.4, containing ammonium sulfate (30% saturation), 10 mM substrate (L-arginine or NOHA), and 1 mM H_4BP at 4°C. The precipitate was rapidly rinsed with 20 mM potassium phosphate buffer, pH 7.4, containing 10 mM substrate (L-arginine or NOHA) and 1 mM H_4BP. Further concentration was achieved by placing the samples on ice under a stream of dry nitrogen gas The entire purification and concentration

processes were performed in 24 h. The resulting samples (~1 mM iron), containing ~30% (v/v) glycerol, were transferred directly to 24 × 3 × 1 mm polycarbonate cuvettes with a Mylar-tape front window and frozen in liquid nitrogen.

The spin state of the nNOS ferriheme used for XAS analysis was checked by EPR spectroscopy. Because holo nNOS is a complex multidomain flavo-metalloenzyme, one of the most difficult steps in the sample preparation is concentration to levels suitable for XAS analysis. Extensive concentration with pressure filtration for extended periods of time often gave nNOS samples with a significantly higher content of high-spin ferric P420 form at g = 6.02 due to disruption of the Fe-S(Cys) bond (*31, 53–55*) and/or low-spin ferriheme species at g = 2.45–2.41, 2.28, and 1.91–1 90, likely due to incomplete water coordination as the axial sixth ligand, as in the case of the concentrated resting enzyme (typically ~30–50%; data not shown). Some of these samples exhibited significant spin-state heterogeneity with respect to the ferriheme site, and thus were unsuitable for XAS analysis (data not shown). On the other hand, ammonium sulfate precipitation in the presence of the substrate and H_4BP gave samples with predominantly high-spin ferriheme species (>90%) exhibiting characteristic EPR spectra (Fig. 1) that were stable during sample manipulation and irradiation at SSRL.

EXAFS analysis was performed with the EXAFSPAK software (courtesy of G.N George; www-ssrl.slac.stanford.edu/exafspak.html) according to standard procedures (*56*) Curve-fitting analysis was performed as described previously by others (*57, 58*). Briefly, the crystallographic coordinates for 2,3,7,8,12,13,17,18-octaethylporphyrinato-iron(II) (*59*) were imported into Chem 3D Pro (Cambridge Scientific) and edited to include only one fourth of porphyrin, excluding hydrogen atoms. The coordinates for the remaining atoms were imported into FEFF v7.02 (*60*) to calculate EXAFS phase and amplitude functions for both single- and multiple-scattering paths. These functions were then incorporated into EXAFSPAK curve-fitting software to fit the data.

TABLE I. **X-ray absorption spectroscopic data collection.**

	Fe EXAFS	Cu EXAFS
SR facility	SSRL	SSRL
Beamlines	7-3, 9-3	7-3, 9-3
Current in storage ring	50–100 mA	50–100 mA
Monochromator crystal	Si[220]	Si[220]
Detection method	fluorescence	fluorescence
Detector type	solid state array[a]	solid state array[a]
Scan length, min	24	26
Scans in average	16	10
Temperature, K	10	10
Energy standard	Fe foil, 1st inflection	Cu foil, 1st inflection
Energy calibration, eV	7,111 2	8,980.3
E_0, eV	7,120	8,990
Pre-edge background		
Energy range, eV	6,852–7,075	8,657–8,945
Gaussian center, eV	6,170	8,040
Width, eV	750	750
Spline background		
Energy range, eV	7,120–7,353 (4)	8,990–9,224 (4)
(Polynomial order)	7,353–7,586 (4)	9,224–9,458 (4)
	7,586–7,819 (4)	9,458–9,691 (4)

[a]The 13-element Ge solid-state X-ray fluorescence detector at SSRL is provided by the NIH Biotechnology Research Resource

RESULTS AND DISCUSSION

EPR Spectra—The resting recombinant mouse nNOS purified in the presence of H_4BP and L-arginine showed citrulline-forming activity of ~220–280 nmol/mg/min at 25°C with an apparent K_m for L-arginine of 1.3 μM (data not shown). A broad Soret band at around 395 nm in the visible absorption spectrum was observed for nNOS in the presence of 0.4 mM L-arginine and 30 μM H_4BP (data not shown) (*31*). The EPR spectrum of the ferriheme center in the resulting enzyme confirms the high-spin species, characterized by apparent g values (g_x = 7.59, g_y = 4.08, and g_z = 1 81) and rhombicity, defined as the ratio of the rhombic and axial zero field splitting parameters, E/D (E/D = 0 073) (Fig. 1A)

Preincubation of the resting enzyme with the intermediate (NOHA) and H_4BP resulted in conversion of the ferriheme species to another different high-spin form with g-values g_x = 7.70, g_y = 3 99, and g_z = 1.80, and greater rhombicity (E/D = 0.077; Fig 1C) The visible absorption spectrum of the NOHA-bound form is indistinguishable from that of the arginine-bound form, displaying a broad Soret band at around 395 nm (data not shown). Thus, the binding of either L-arginine or NOHA causes an EPR-detectable local conformational change in the enzyme that produces ligand-specific high-spin species (*20*). The narrow linewidths of the EPR spectra suggest that the substrate target atom in high-spin ferric nNOS is located at a well-ordered position near to the ferriheme iron. The geometry and

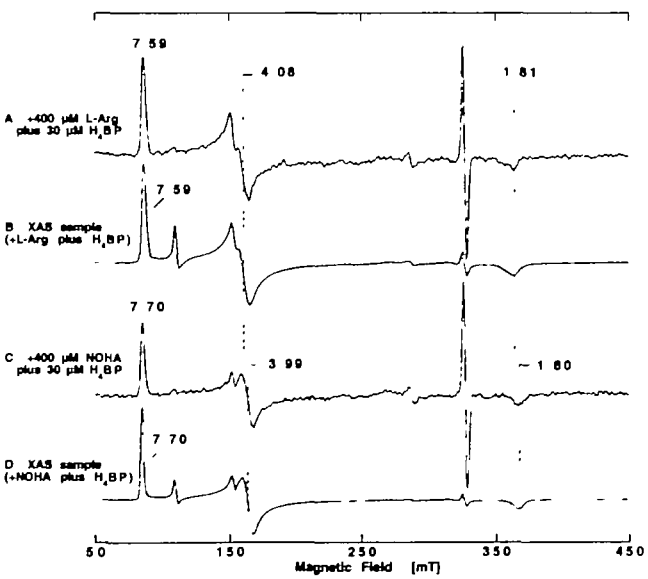

Fig 1. **EPR spectra at 7 K of L-arginine-bound (A) and NOHA-bound nNOS (C), and the XAS samples of L-arginine-bound (B) and NOHA-bound nNOS (D).** All nNOS samples used in this work were purified in the presence of H_4BP cofactor. The minor ferriheme species at g = 6 02 (less than 2–3% of the total ferriheme) was formed during concentration of the nNOS samples. A signal at g = 4 3 from high-spin rhombic Fe^{3+} represents a small amount of adventitiously bound non-heme iron The loss of a radical feature at g = 2 0 for the XAS samples is due to the long-term storage of the samples at cryogenic temperature (below –80°C). Instrument settings microwave power, 1 mW, modulation amplitude, 1 mT; variable gain; the g values are indicated in the figure.

structures of these high-spin ferriheme species were further investigated by X-ray absorption spectroscopy.

Fe K-Edge XAS Analysis—The similarity between the Fe K-edge X-ray absorption spectra of the NOHA- and arginine-bound forms (Fig. 2A) implies a general structural and electronic equivalence between the iron coordination sites of the two forms. The Fe EXAFS for L-arginine-bound nNOS are best fit assuming a sulfur ligand at 2.30 Å and four nitrogen atoms (from the plane of porphyrin) at 2 03 Å (Fit 1; Table II and Fig. 3A), while the EXAFS for NOHA-bound nNOS are best fit assuming a sulfur atom at 2.29 Å and four porphyrin nitrogen atoms at 2.02 Å (Fit 2; Table II and Fig. 3B).

Fe K-edge EXAFS of the high-spin ferric states of cytochrome $P450_{cam}$ and chloroperoxidase shows the presence of a sulfur donor ligand coordinated to the iron at 2.23–2.26 and 2.30 Å, respectively (*37–40*). The observed Fe-S bond distances (2.29 Å) of full-length nNOS and chloroperoxidase are longer than that of high-spin ferric cytochrome $P450_{cam}$, but shorter than those of known Fe(III)-S(thiolate) heme iron model systems (*37–39*)

Effect of a Divalent Cation Inhibitor on the Iron Coordination Environment of nNOS—It has been reported that constitutive NOS activity in rat cerebellum is inhibited by several divalent cations, such as Cu^{2+}, Pb^{2+}, and Zn^{2+} (*44*). Cu^{2+} uptake by glial cells selectively inhibits nNOS activity, and results in a decrease of the basal intracellular cGMP levels and an increase of iNOS-mediated NO synthesis through transcriptional activation of iNOS mRNA (*61*). Cu^{2+} also suppresses the eNOS activity extracted from pulmonary arterial endothelial cells (*45*), but in the presence of extracellular Ca^{2+}, it relaxes vessels and results in the accumulation of eNOS-mediated cGMP in the pulmonary artery employing extrapulmonary arterial rings (*62*). The Cu^{2+}-mediated increase of NO production *via* eNOS activation is due to Ca^{2+} influx into the pulmonary arterial endothelial cells (*45, 63*). Thus, Cu^{2+} has been proposed to play regulatory roles in controlling NOS and guanylyl cyclase activity in mammalian cells.

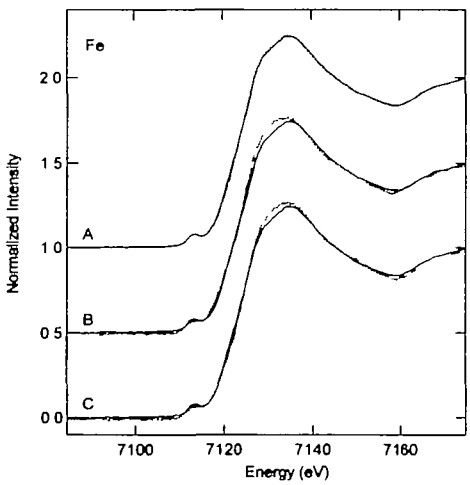

Fig. 2. **Fe K-edge X-ray absorption spectra for L-arginine-bound nNOS ferriheme (A, B, C; solid) compared with NOHA-bound nNOS (A; dashed), L-arginine-bound nNOS containing 1 eq. Cu^{2+} (per heme) (B; dashed), or L-arginine-bound nNOS incubated with excess (*ca.* 2 eq.) Cu^{2+} (C; dashed).**

We confirmed that several divalent cations, such as the Cu^{2+}, Mn^{2+}, and Zn^{2+} ions, at 1 mM completely inhibit nNOS activity (data not shown). It has been reported that the Zn^{2+} ion perturbs the environment of the heme iron in nNOS (*64*), and Perry and Marletta (*46*) have postulated that exogenous Fe^{2+} might bind in close proximity to the heme and/or H_4BP center of NOS. We therefore examined the effect of Cu^{2+} on the immediate heme coordination environment of nNOS by X-band EPR, and Cu and Fe K-edge XAS The XAS technique "sees" the average coordination environment of all atoms of a given element, and is suitable for analyzing any structural changes of the nNOS metal centers upon Cu^{2+} binding. The effect of exogenous Zn^{2+} or Fe^{2+} was not investigated in this study because of the presence of a tetrahedral tetrathiolate zinc center at the dimer interface and heme iron in NOS oxygenase domains (*10, 11, 13, 43, 65*).

The Cu^{2+}-inhibited form of arginine/H_4BP-bound nNOS yields high-spin ferriheme EPR signals that are similar to those observed for arginine/H_4BP-bound nNOS (Fig. 4). An additional broad Cu^{2+} signal is also observed in the $g = 2$ region. The difference between the line positions of the high-spin ferriheme in the absence and presence of Cu^{2+} is less than the line widths. The presence of the low-spin ferriheme signals at $g = 2.41$, 2.28, and 1.91 for the Cu^{2+}-inhibited forms indicates that a small amount of low-spin ferriheme is formed in the presence of excess Cu^{2+} ion (Fig. 5), as was previously reported for inhibition of nNOS by Zn^{2+} (*64*). However, the observable spin state conversion of the nNOS ferriheme with the Cu^{2+} ion was minimal (estimated to be approximately 15% of the total ferriheme) even in the presence of a saturating amount of Cu^{2+}, and the degree of the spin state conversion is not consistent with

TABLE II **Curve fitting results for Fe EXAFS.**[a]

Sample, $\Delta k^3\chi$ filename (k range)	Fit	Shell	R_{ss} (Å)	σ_{ss}^2 (Å^2)	f'[a]
nNOS + L-Arg, $\Delta k^3\chi$ = 14 26[a]	1	Fe-S	2 30	0.0021	0 074
NOSRB (2–11.5 Å^{-1})		Fe-N_4	2.03	0.0028	
nNOS + L-ArgOH, $\Delta k^3\chi$ = 14 26	2	Fe-S	2 29	0 0015	0 072
NOSHB (2–11 5 Å^{-1})		Fe-N_4	2.02	0 0037	
nNOS + L-Arg + 1eq Cu^{2+}, $\Delta k^3\chi$ = 13 43	3	Fe-S	2 29	0 0018	0 093
FNABA (2–11 5 Å^{-1})		Fe-N_4	2 00	0 0033	
nNOS + L-Arg + excess Cu^{2+}, $\Delta k^3\chi$ = 14 59	4	Fe-S	2 28	0 0031	0.103
FNACA (2–11 5 Å^{-1})		Fe-N_4	2 00	0 0036	

R_{ss} is the metal-scatterer distance. σ_{ss}^2 is a mean square deviation in R_{ss}. [a]f' is a normalized error (chi-squared):

$$f' = \frac{\{\Sigma_i[k^3(\chi_i^{obs} - \chi_i^{calc})]^2 / N\}^{1/2}}{\Delta k^3 \chi}.$$

the total loss of the citrulline formation activity.

Fe K-edge XAS indicates that the addition of excess Cu^{2+} only slightly affects the immediate ferriheme coordination environment (Fig. 2, B and C). There is no evidence of Fe-Cu (Fig. 3) or Cu-Fe scattering in the EXAFS and FT spectra. Furthermore, Cu K-edge absorption spectra and EXAFS (data not shown) indicate that nNOS-bound Cu^{2+} ions are indistinguishable from spectra recorded in the presence of excess Cu^{2+}, and no evidence for the hyperfine coupling of Cu^{2+} with ^{14}N nuclei was obtained by EPR (Figs. 4 and 5). Thus, the Cu^{2+} inhibition slightly affects the spin-state equilibrium but causes no significant change in the immediate ferriheme coordination environment of nNOS. Contrary to the earlier proposals by others (*46, 64*), these results suggest that the Cu^{2+} responsible for the inhibitory effect binds away from the heme site to cause a slight conformational change and to block the citrulline formation activity

NOS isoforms are compex multidomain proteins with multiple redox centers, whose overall conformation is highly sensitive to binding of substrates and cofactors such as H_4BP, which binds in close proximity to the heme site (*10–13, 43*). Because XAS indicates that the divalent metal does not bind near the heme, our results provide no support for the aromatic amino acid hydroxylase reaction of H_4BP in nNOS catalysis, which would require a non-heme iron center in close proximity to the H_4BP center. This is in line with other indirect evidence inferred from recent studies (*43, 66, 67*).

Structure of the High-Spin Ferriheme Site in Substrate-bound nNOS—Central to all proposed catalytic mechanisms for the two-step oxygenase reaction by NOS isoforms is the close proximity of the reactive guanidino nitrogen of the substrate to the heme iron. The present XAS analysis demonstrates that the high-spin ferriheme site geometry and Fe-S(thiolate) bond distances of the arginine-bound and NOHA-bound forms of full-length nNOS in the presence of H_4BP are essentially identical, with a Fe-S(thiolate) bond distance of 2 30 Å, indicating no significant stretching of the Fe-S (thiolate) bond between the two high-spin ferric forms (Fig. 6). The substrate is not a ligand to the high-spin, five-coordinate ferriheme iron of full-length nNOS, consistent with inferences based on the results obtained with other spectroscopic techniques (*17–22, 24–26*). These structural features are in good agreement with the previously reported crystal structures of the arginine-bound eNOS and iNOS oxygenase domains in the presence of H_4BP [showing the presence of a cysteinate ligand with a

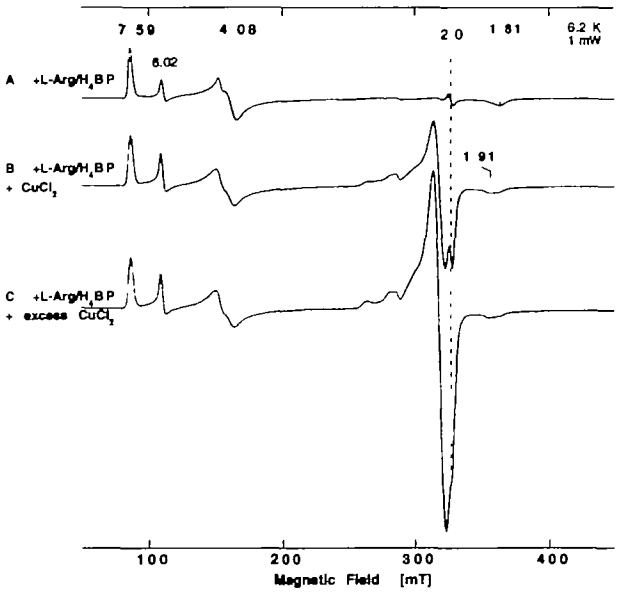

Fig 4 **EPR spectra at 6.2 K of the high-spin ferriheme center of L-arginine bound nNOS in the presence of H_4BP (A), and in the presence of 1 eq. Cu^{2+} (B) or excess (*ca.* 2 eq.) Cu^{2+} (C).** Instrument settings microwave power, 1 mW; modulation amplitude, 1 mT, the *g* values are indicated in the figure

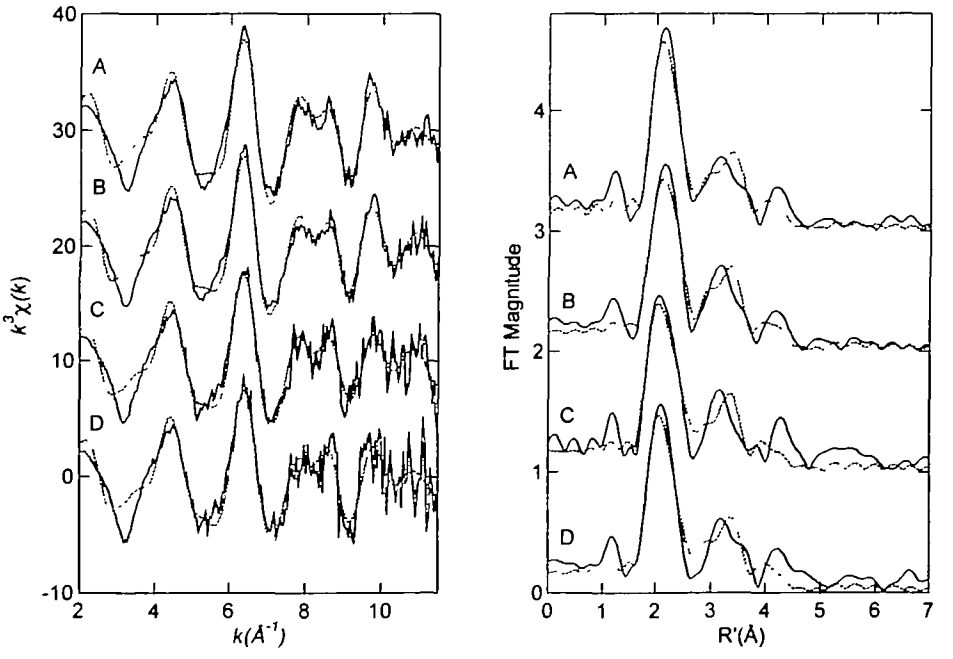

Fig 3 **X-ray absorption fine structure (left) and Fourier transforms (right, over k=2–11.5 $Å^{-1}$) for L-arginine–bound nNOS ferriheme (A, solid) compared with the calculated spectra for Fit 1, Table II (A; dashed), NOHA-bound nNOS (B, solid) compared with the calculated spectra for Fit 2, Table II (B; dashed), L-arginine–bound nNOS containing 1 eq. Cu^{2+} (per total heme) (C; solid) compared with the calculated spectra for Fit 3, Table II (C; dashed), or L-arginine–bound nNOS containing excess (*ca.* 2 eq.) Cu^{2+} (D; solid) compared with the calculated spectra for Fit 4, Table II (D; dashed).**

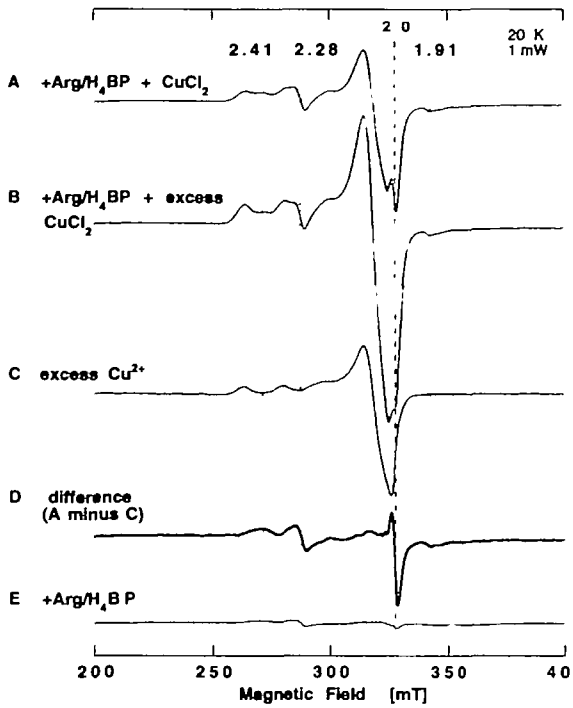

Fig 5 **EPR spectra at 20 K of L-arginine bound nNOS in the presence of H_4BP (E), and in the presence of 1 eq. Cu^{2+} (A) or excess (*ca.* 2 eq.) Cu^{2+} (B). Subtraction of spectrum A from B gives an EPR spectrum attributed to adventitiously bound Cu^{2+} (C), and subtraction of resulting spectrum C from A or B gives an identical EPR spectrum attributed to the minor low-spin ferriheme species of nNOS (D).** The EPR samples used are the same as those in Fig 2 Instrument settings microwave power, 1 mW, modulation amplitude, 1 mT; the *g* values are indicated in the figure

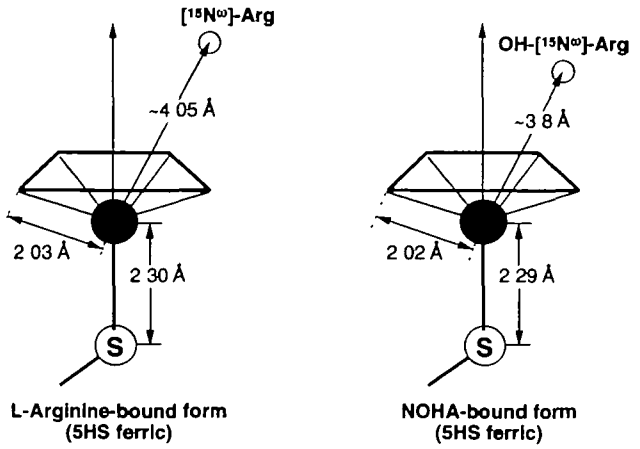

Fig 6 **Schematic illustration of the heme site geometry of L-arginine (A) and NOHA (B) bound nNOS ferriheme.** This illustration is based on the structural information on the high-spin ferriheme coordination environment of the ligand-bound full-length nNOS obtained through the present XAS analysis, and the Q-band pulsed ^{15}N ENDOR analysis by Tierney *et al* (*69, 70*).

Fe-S distance of about 2 3 Å (*11–13, 43, 68*)], and the iNOS oxygenase domain complexed with NOHA (reported during the preparation of this paper (*68*)), and therefore likely common among the NOS isoforms. In the 2.4-Å resolution crystal structure of the human eNOS oxygenase domain, the iron was found to be 0.65 Å out of the plane of the four pyrrole nitrogens toward the cysteinate ligand (*11*). Interestingly, the Fe-S (thiolate) bond length of full-length nNOS is similar to that of the high-spin ferric state of chloroperoxidase, but longer than that of cytochrome $P450_{cam}$ (*37–39*). This seems to be in line with the results of previous resonance Raman analysis of the ferrous CO-bound forms of substrate-bound nNOS by Wang *et al.* (*24*), suggesting that the bonding of the cysteinate to the heme iron may be weaker, as observed in chloroperoxidase, than in cytochrome $P450_{cam}$, on the basis of the inverse correlation between the Fe-CO and C-O stretching modes.

Finally, the absence of XAS-detectable differences in the heme site structure and geometry or the conformation of the enzyme-bound substrate between the L-arginine– and NOHA-bound forms indicates that the position of the reactive guanidino nitrogen (N^{ω}) of L-arginine and NOHA in the binding site, and the resulting orientation of the ferrous-O_2 adduct, rather than the heme site structure and geometry, specify the two-step hydroxylation reactions in the catalytic site of full-length nNOS. The position of the reactive guanidino nitrogen (N^{ω}) of L-arginine and the hydroxylated nitrogen of NOHA relative to the high-spin ferriheme iron of full-length nNOS has been determined by very recent Q-band pulsed ^{15}N ENDOR analysis, which showed that $^{15}N^{\omega}$ of singly labeled NOHA at the hydroxylated nitrogen is 3.8 Å from the ferriheme iron, *i.e.* closer than the corresponding guanidino $^{15}N^{\omega}$ of L-arginine (4.05 Å) (*69, 70*). In conjunction with the common structure and geometry of the high-spin ferriheme site of the substrate-bound nNOS revealed in this study, it can be concluded that the high-spin ferric nNOS holds the substrate target atom in a well-ordered position near the heme iron (Fig 6), which may be favorably located for subsequent hydroxylation by an iron-bound oxygenic species. Further XAS analysis with different oxidation and spin-states of nNOS, along with other analytical techniques, will firmly establish the detailed structural changes of the heme site geometry and the reaction intermediates in the catalytic events of NOS isoforms.

We wish to thank Drs. K. Tamura and T. Iizuka (The Institute of Physical and Chemical Research) for allowing us to utilize the X-band EPR facility, Dr T Oshima (Tokyo University of Pharmacy and Life Science) for allowing us access to the large-scale fermenter facility, and Y Hayashi (Nippon Medical School) for the excellent technical assistance We also thank Marion Cosper for the help in acquiring some of the XAS data

REFERENCES

1. Griffith, O. and Stuehr, D.J. (1995) Nitric oxide synthases. properties and catalytic mechanism *Annu Rev. Physiol.* **57**, 707–736
2. Ignarro, L J. (1996) Physiology and pathophysiology of nitric oxide. *Kidney Int.* **55**, S2–S5
3. Marletta, M.A. (1994) Nitric oxide synthase aspects concerning structure and catalysis. *Cell* **78**, 927–930
4 Moncada, S and Higgs, E.A. (1995) Molecular mechanisms and therapeutic strategies related to nitric oxide. *FASEB J* **9**, 1319–1330
5 Nathan, C. and Xie, Q -w. (1994) Regulation of biosynthesis of nitric oxide *J Biol Chem.* **269**, 13725–13728
6. Stuehr, D.J (1999) Mammalian nitric oxide synthases. *Bio-*

chim Biophys. Acta **1411**, 217–230
7 Stuehr, D J (1997) Structure-function aspects in the nitric oxide synthases. *Annu Rev. Pharmacol* **37**, 339–359
8 Masters, B S S, McMillan, K., Sheta, E.A., Nishimura, J.S., Roman, L J., and Martásek, P (1996) Neuronal nitric oxide synthase, a modular enzyme formed by convergent evolution structure studies of a cysteine thiolate-liganded heme protein that hydroxylates L-arginine to produce NO as a cellular signal *FASEB J* **10**, 552–558
9 Knowles, R G and Moncada, S (1994) Nitric oxide synthases in mammals *Biochem. J* **298**, 249–258
10. Crane, B R, Rosenfeld, R J, Arvai, A S, Ghosh, D K., Ghosh, S, Tainer, J.A., Stuehr, D J, and Getzoff, E D (1999) N-terminal domain swapping and metal ion binding in nitric oxide synthase dimerization *EMBO J* **18**, 6271–6281
11. Fischmann, T O., Hruza, A., Niu, X.D, Fossetta, J D, Lunn, C.A., Dolphin, E, Prongay, A.J, Reichert, P, Lundell, D J, Narula, S K., and Weber, P C (1999) Structural characterization of nitric oxide synthase isoforms reveals striking active-site conservation *Nat Struct Biol* **6**, 233–242
12. Crane, B.R., Arvai, A.S., Ghosh, D K., Wu, C, Getzoff, E D, Stuehr, D J, and Tainer, J A. (1998) Structure of nitric oxide synthase oxygenase dimer with ptein and substrate. *Science* **279**, 2121–2126
13 Raman, C S, Li, H, Martásek, P, Král, V., Masters, B S S, and Poulos, T L. (1998) Crystal structure of constitutive endothelial nitric oxide synthase a paradigm for ptein function involving a novel metal center *Cell* **95**, 939–950
14 Marletta, M.A. (1993) Nitric oxide synthase structure and mechanism *J Biol Chem* **268**, 12231–12234
15 Abu-Soud, H M, Gachhui, R, Raushel, F M, and Stuehr, D J (1997) The ferrous-dioxy complex of neuronal nitric oxide synthase divergent effects of L-arginine and tetrahydrobiopterin on its stability *J Biol Chem* **272**, 17349–17353
16 Ledbetter, A.P, McMillan, K., Roman, L J, Masters, B S S., Dawson, J H, and Sono, M (1999) Low-temperature stabilization and spectroscopic characterization of the dioxygen complex of the ferrous neuronal nitric oxide synthase oxygenase domain *Biochemistry* **38**, 8014–8021
17 Stuehr, D J and Ikeda-Saito, M. (1992) Spectral characterization of brain and macrophage nitric oxide synthases cytochrome P-450-like hemoproteins that contain a flavin semiquinone radical *J Biol Chem* **267**, 20547–20550
18. Wang, J, Stuehr, D J, Ikeda-Saito, M, and Rousseau, D L (1993) Heme coordination and structure of the catalytic site in nitric oxide synthase *J Biol Chem.* **268**, 22255–22258
19 Sono, M, Stuehr, D J, Ikeda-Saito, M, and Dawson, J H (1995) Identification of nitric oxide synthase as a thiolate-ligand heme protein using magnetic circular dichroism spectroscopy· comparison with cytochrome P-450-cam and chloroperoxidase *J Biol Chem* **270**, 19943–19948
20 Salerno, J C, McMillan, K., and Masters, B S S (1996) Binding of intermediate, product, and substrate analogs to neuronal nitric oxide synthase ferriheme is sensitive to ligand-specific effects in the L-arginine binding site. *Biochemistry* **35**, 11839–11845
21 Galli, C, MacArthur, R., Abu-Soud, H M, Clark, P, Steuhr, D J, and Brudvig, G.W (1996) EPR spectroscopic characterization of neuronal NO synthase. *Biochemistry* **35**, 2804–2810
22 Tsai, A.-L., Berka, V., Chen, P-F., and Palmer, G (1996) Characterization of endothelial nitric-oxide synthase and its reaction with ligand by electron paramagnetic resonance spectroscopy *J Biol Chem.* **271**, 32563–32571
23. Poulos, T L. (1996) The role of the proximal ligand in heme enzymes *J Biol Inorg. Chem.* **1**, 356–359
24 Wang, J, Stuehr, D.J., and Rousseau, D L (1997) Interactions between substrate analogues and heme ligands in nitric oxide synthase *Biochemistry* **36**, 4595–4606
25 Migita, C.T., Salerno, J.C, Masters, B S.S, Martásek, P, McMillan, K., and Ikeda-Saito, M (1997) Substrate binding-induced changes in the EPR spectra of the ferrous nitric oxide complexes of neuronal nitric oxide synthase. *Biochemistry* **36**, 10987–10992
26. Fan, B, Wang, J, Stuehr, D, and Rousseau, D L (1997) NO synthase isozymes have distinct substrate binding sites. *Biochemistry* **36**, 12660–12665
27 Iwanaga, T., Yamazaki, T, and Kominami, S (1999) Kinetic studies on the successive reaction of neuronal nitric oxide synthase from L-arginine to nitric oxide and L-citrulline. *Biochemistry* **38**, 16629–16635
28 Sono, M., Roach, M P, Coulter, E D, and Dawson, J H (1996) Heme-containing oxygenases. *Chem Rev.* **96**, 2841–2887
29 Klatt, P, Schmidt, K., Lehner, D., Glatter, O., Bachinger, H P., and Mayer, B (1995) Structural analysis of porcine brain nitric oxide synthase reveals a role for tetrahydrobiopterin and L-arginine in the formation of an SDS-resistant dimer. *EMBO J* **14**, 3687–3695
30 Rodríguez-Crespo, I, Moénne-Loccoz, P, Loehr, T M., and Ortiz de Montellano, P.R (1997) Endothelial nitric oxide synthase modulations of the distal heme site produced by progressive N-terminal deletions. *Biochemistry* **36**, 8530–8538
31 Iwasaki, T, Hori, H, Hayashi, Y., and Nishino, T. (1999) Modulation of the remote heme site geometry of recombinant mouse neuronal nitric oxide synthase by the N-terminal hook region *J Biol. Chem* **274**, 7705–7713
32 Ghosh, D K., Crane, B R, Ghosh, S, Wolan, D, Gachhui, R, Crooks, C, Presta, A., Tainer, J.A., Getzoff, E D, and Stuehr, D J (1999) Inducible nitric oxide synthase role of the N-terminal β-hairpin hook and ptein-binding segment in dimerization and tetrahydrobiopterin interaction *EMBO J* **18**, 6260–6270
33 Kwon, N S, Nathan, C F, and Stuehr, D J (1989) Reduced biopterin as a cofactor in the generation of nitrogen oxides by murine macrophages *J Biol Chem.* **264**, 20496–20501
34 Stuehr, D J, Kwon, N S, Nathan, C F, Griffith, O.W, Feldman, P L, and Wiseman, J (1991) N^{ω}-hydroxy-L-arginine is an intermediate in the biosynthesis of nitric oxide from L-arginine *J Biol Chem* **266**, 6259–6263
35 Witteveen, C F B, Giovanelli, J, and Kaufman, S (1999) Reactivity of tetrahydrobiopterin bound to nitric-oxide synthase. *J Biol Chem* **274**, 29755–29762
36 Hurshman, A.R, Krebs, C, Edmondson, D.E, Huynh, B H, and Marletta, M.A. (1999) Formation of a ptein radical in the reaction of the heme domain of inducible nitric oxide synthase with oxygen *Biochemistry* **38**, 15689–15696
37 Dawson, J H and Sono, M (1987) Cytochrome P-450 and chloroperoxidase thiolate-ligated heme enzymes spectroscopic determination of their active site structures and mechanistic implications of thiolate ligation *Chem Rev* **87**, 1255–1276
38 Cramer, S P, Dawson, J H, Hodgson, K.O, and Hager, L.P (1978) Studies on the ferric forms of cytochrome P-450 and chloroperoxidase by extended X-ray absorption fine structure characterization of the Fe-N and Fe-S distances *J Am Chem Soc.* **100**, 7282–7290
39 Hahn, J.E., Hodgson, K.O, Andersson, L.A., and Dawson, J H (1982) Endogenous cysteine ligation in ferric and ferrous cytochrome P-450 direct evidence from X-ray absorption spectroscopy *J Biol Chem.* **257**, 10934–10941
40 Obayashi, E, Tsukamoto, K., Adachi, S-i., Takahashi, S., Nomura, M, Iizuka, T, Shoun, H, and Shiro, Y. (1997) Unique binding of nitric oxide to ferric nitric oxide reductase from Fusarium oxysporum elucidated with infrared, resonance Raman, and X-ray absorption spectroscopies. *J Am Chem Soc.* **119**, 7807–7816
41 Shiro, Y., Sato, F., Suzuki, T, Iizuka, T, Matsushita, T., and Oyanagi, H. (1990) X-ray absorption spectral study of ferric high-spin hemoproteins. XANES evidences for coordination structure of the heme iron. *J. Am Chem Soc.* **112**, 2921–2924
42 Liu, H I., Sono, M, Kadkhodayan, S, Hager, L P, Hedman, B, Hodgson, K.O, and Dawson, J H. (1995) X-ray absorption near edge studies of cytochrome P-450-CAM, chloroperoxidase, and myoglobin. direct evidence for the electron releasing character of a cysteine thiolate proximal ligand. *J Biol. Chem* **270**, 10544–10550
43 Li, H., Raman, C S, Glaser, C B., Blasko, E., Young, T A., Par-

kinson, J.F., Whitlow, M., and Poulos, T.L. (1999) Crystal structures of zinc-free and -bound heme domain of human inducible nitric-oxide synthase. *J. Biol. Chem.* **274**, 21276–21284
44. Quinn, M.R. and Harris, C.L. (1995) Lead inhibits Ca^{2+}-stimulated nitric oxide synthase activity from rat cerebellum. *Neurosci. Lett.* **196**, 65–68
45. Demura, Y., Ameshima, S., Ishizaki, T., Okamura, S., Miyamori, I., and Matsukawa, S. (1998) The activation of eNOS by copper ion (Cu^{2+}) in human pulmonary arterial endothelial cells (HPAEC). *Free Radic. Biol. Med.* **25**, 314–320
46. Perry, J.M. and Marletta, M.A. (1998) Effects of transition metals on nitric oxide synthase catalysis. *Proc. Natl. Acad. Sci. U.S.A.* **95**, 11101–11106
47. Muchmore, D.C., McIntosh, L.P., Russell, C.B., Anderson, D.E., and Dahlquist, F.W. (1989) Expression and nitrogen-15 labeling of proteins for proton and nitrogen-15 nuclear magnetic resonance. *Methods Enzymol.* **177**, 44–73
48. Gerber, N.C., and Ortiz de Montellano, P.R. (1995) Neuronal nitric oxide synthase expression in *Escherichia coli*, irreversible inhibition by phenyldiazene, and active site topology. *J. Biol. Chem.* **270**, 17791–17796
49. Roman, L.J., Sheta, E.A., Martásek, P., Gross, S.S., Liu, Q., and Masters, B.S.S. (1995) High-level expression of functional rat neuronal nitric oxide synthase in *Escherichia coli*. *Proc. Natl. Acad. Sci. USA* **92**, 8428–8432
50. Hori, H., Iwasaki, T., Kurahashi, Y., and Nishino, T. (1997) Calcium-dependent inactivation of neuronal nitric oxide synthase: evidence for the existence of stabilization/activation factor. *Biochem. Biophys. Res. Commun.* **234**, 476–480
51. Iwasaki, T., Wakagi, T., Isogai, Y., Tanaka, K., Iizuka, T., and Oshima, T. (1994) Functional and evolutionary implications of a [3Fe-4S] cluster of the dicluster-type ferredoxin from the thermoacidophilic archaeon, *Sulfolobus* sp. strain 7. *J. Biol. Chem.* **269**, 29444–29450
52. Fann, Y.C., Ahmed, I., Blackburn, N.J., Boswell, J.S., Verkhovskaya, M.L., Hoffman, B.M., and Wikström, M. (1995) Structure of CuB in the binuclear heme-copper center of the cytochrome aa_3-type quinol oxidase from *Bacillus subtilis* an ENDOR and EXAFS study. *Biochemistry* **34**, 10245–10255
53. Wang, J., Stuehr, D.J., and Rousseau, D.L. (1995) Tetrahydrobiopterin-deficient nitric oxide synthase has a modified heme environment and forms a cytochrome P-420 analog. *Biochemistry* **34**, 7080–7087
54. Iwasaki, T., Hori, H., Hayashi, Y., Nishino, T., Tamura, K., Oue, S., Iizuka, T., Ogura, T., and Esumi, H. (1999) Characterization of mouse nNOS2, a natural variant of neuronal nitric-oxide synthase produced in the central nervous system by selective alternative splicing. *J. Biol. Chem.* **274**, 17559–17566
55. Huang, L., Abu-Soud, H.M., Hille, R., and Stuehr, D.J. (1999) Nitric oxide-generated P420 nitric oxide synthase: characterization and roles for tetrahydrobiopterin and substrate in protecting against or reversing the P420 conversion. *Biochemistry* **38**, 1912–1920
56. Scott, R.A. (1985) Measurement of metal-ligand distances by EXAFS. *Methods Enzymol.* **117**, 414–459
57. Rich, A.M., Armstrong, R.S., Ellis, P.J., Freeman, H.C., and Lay, P.A. (1998) Determination of iron-ligand bond lengths in horse heart Met- and deoxymyoglobin using multiple-scattering XAFS analyses. *Inorg. Chem.* **37**, 5743–5753
58. Rich, A.M., Armstrong, R.S., Ellis, P.J., and Lay, P.A. (1998) Determination of the Fe-ligand bond lengths and Fe-N-O bond angles in horse heart ferric and ferrous nitrosylmyoglobin using multiple-scattering XAFS analysis. *J. Am. Chem. Soc.* **120**, 10827–10836
59. Strauss, S.H., Silver, M.E., Long, K.M., Thompson, R.G., Hudgens, R.A., Spartalian, K., and Ibers, J.A. (1985) Comparison of the molecular and electronic-structures (2,3,7,8,12,13,17,18-octaethylporphyrinato)iron(II) and (trans-7,8-dihydro-2,3,7,8,12,13,17,18-octaethylporphyrinato)iron(II). *J. Am. Chem. Soc.* **107**, 4207
60. Zabinsky, S.I., Rehr, J.J., Ankudinov, A., Albers, R.C., and Eller, M.J. (1995) Multiple-scattering calculations of X-ray absorption spectra. *Phys. Rev.* **B52**, 2995–3009
61. Colasanti, M., Persichini, T., Venturini, G., Polticelli, F., and Musci, G. (2000) Modulation of the nitric oxide pathway by copper in glial cells. *Biochem. Biophys. Res. Commun.* **275**, 776–782
62. Ohnishi, T., Ishizaki, T., Sasaki, F., Ameshima, S., Nakai, T., Miyabo, S., and Matsukawa, S. (1997) The effect of Cu^{2+} on rat pulmonary arterial rings. *Eur. J. Pharmacol.* **319**, 49–55
63. Demura, Y., Ishizaki, T., Ameshima, S., Okamura, S., Hayashi, T., Matsukawa, S., and Miyamori, I. (1998) The activation of nitric oxide synthase by copper ion is mediated by intracellular Ca^{2+} mobilization in human pulmonary arterial endothelial cells. *Br. J. Pharmacol.* **125**, 1190–1197
64. Persechini, A., McMillan, K., and Masters, B.S.S. (1995) Inhibition of nitric synthase activity by Zn^{2+} ion. *Biochemistry* **34**, 15091–15095
65. Miller, R.T., Martásek, P., Raman, C.S., and Masters, B.S.S. (1999) Zinc content of *Escherichia coli*-expressed constitutive isoforms of nitric-oxide synthase. *J. Biol. Chem.* **274**, 14537–14540
66. Rodríguez-Crespo, I., Nishida, C.R., Knudsen, G.M., and Ortiz de Montellano, P.R. (1999) Mutation of the five conserved histidines in the endothelial nitric-oxide synthase hemoprotein domain: no evidence for a non-heme metal requirement for catalysis. *J. Biol. Chem.* **274**, 21617–21624
67. Perry, J.M., Zhao, Y., and Marletta, M.A. (2000) Cu^{2+} and Zn^{2+} inhibit nitric-oxide synthase through an interaction with the reductase domain. *J. Biol. Chem.* **275**, 14070–14076
68. Crane, B.R., Arvai, A.S., Ghosh, S., Getzoff, E.D., Stuehr, D.J., and Tainer, J.A. (2000) Structure of the Nw-hydroxy-L-arginine complex of inducible nitric oxide synthase oxygenase dimer with active and inactive pterins. *Biochemistry* **39**, 4608–4621
69. Tierney, D.L., Martásek, P., Doan, P.E., Masters, B.S.S., and Hoffman, B.M. (1998) Location of guanidino nitrogen of L-arginine substrate bound to neuronal nitric oxide synthase (nNOS) determination by Q-band pulsed ENDOR spectroscopy. *J. Am. Chem. Soc.* **120**, 2983–2984
70. Tierney, D.L., Huang, H., Martásek, P., Masters, B.S.S., Silverman, R.B., and Hoffman, B.M. (1999) ENDOR spectroscopic evidence for the position and structure of N^G-hydroxy-L-arginine bound to holo-neuronal nitric oxide synthase. *Biochemistry* **38**, 3704–3710